SAND2014-0076C

Toward Transition Statistics Measured on a 7-Degree Hypersonic Cone for Turbulent Spot Modeling

Katya M. Casper*, Steven J. Beresh†, John F. Henfling‡, and Russell W. Spillers§
Sandia National Laboratories, Albuquerque, NM 87185

High-frequency pressure sensors were used in conjunction with a high-speed schlieren system to study the growth and breakdown of boundary-layer disturbances into turbulent spots on a 7° cone in the Sandia Hypersonic Wind Tunnel at Mach 5 and 8. To relate the intermittent disturbances to the average characteristics of transition on the cone, the statistical distribution of these disturbances must be known. These include the boundary-layer intermittency, burst rate, and average disturbance length.

Traditional low-speed methods to characterize intermittency identify only turbulent/non-turbulent regions. However at high M, instability waves become an important part of the transitional region. Algorithms to distinguish instability waves from turbulence in both the pressure and schlieren measurements have been developed and the corresponding intermittency, burst rate, and average burst length of both regions have been computed for several cases at Mach 5 and 8. Work continues to develop these algorithms and determine the sensitivity of the transition statistics to threshold values inherent to the algorithms. Distinguishing instability waves from turbulence gives a better description of the intermittent boundary layer at high M and will allow the fluctuations associated with boundary-layer instabilities to be incorporated into transitional models.

Nomenclature

δ	boundary-layer thickness (mm)	R	cone radius (mm)
f	frequency (kHz)	Re	freestream unit Reynolds number (1/m)
M	freestream Mach number	t	time (s)
P_0	tunnel stagnation pressure (kPa)	T_0	tunnel stagnation temperature (K)
p'	pressure fluctuation, $p - p_e$ (Pa)	x	axial model coordinate measured from nose (m)
p_e	boundary-layer edge pressure (Pa)		

I. Introduction

Hypersonic reentry vehicles are subjected to high levels of fluctuating pressures. These intense fluctuations can cause vibration of internal components and lead to structural problems. There is a need to predict the magnitude, frequency content, location, and spatial extent of the pressure fluctuations to better design hypersonic flight vehicles. Current designs often use overly conservative estimates of the fluctuations which lead to heavier vehicles and degraded flight performance. Some correlations exist for the magnitude of transitional and turbulent pressure fluctuations, but these were derived primarily using either incompressible data or conventional (noisy flow) hypersonic wind-tunnel tests.[1] Such modeling efforts have not led to sufficient physical understanding of the transitional pressure fluctuations or to adequate predictive capabilities.

*Senior Member of the Technical Staff, Engineering Sciences Center, Member AIAA, kmcaspe@sandia.gov, (505) 844-1574
†Principal Member of the Technical Staff, Engineering Sciences Center, Associate Fellow AIAA
‡Distinguished Technologist, Member AIAA
§Principal Technologist

Sandia National Laboratories is a multi-program laboratory managed and operated by Sandia Corporation, a wholly owned subsidiary of Lockheed Martin Corporation, for the U.S. Department of Energy's National Nuclear Security Administration under contract DE-AC04-94AL85000.

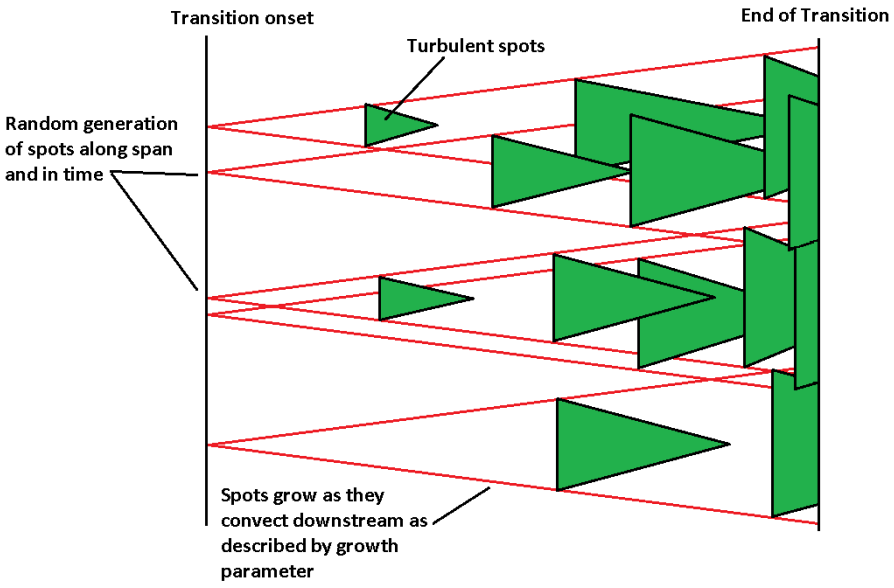

Figure 1. Schematic of turbulent-spot model of transition.

Modern computational capabilities seem likely to enable higher-fidelity models in the future if they have a better scientific basis on which to build.

During boundary-layer transition, the heating rates and pressure fluctuations that are experienced are higher than for a fully turbulent boundary layer.[2–6] These high pressure fluctuations result from repeated intermittent spatial-temporal switching between laminar and turbulent regions, creating a broad spectrum of disturbances. Unfortunately in flight, natural transition typically occurs over a large portion of the vehicle,[7] making transitional fluctuations of primary interest for this work.

The transition process can be described through intermittency and the growth and propagation of turbulent spots in the transitional boundary layer.[8,9] Fig. 1 shows a schematic of this model, though with far fewer turbulent spots than a real transition scenario. The model assumes concentrated breakdown in which the turbulent spots are generated near a single streamwise location. The spots are randomly generated along the span and in time. Upstream and downstream of transition onset, no new spots are generated. A spot growth parameter describes the lateral and streamwise growth of the spots as they convect downstream. There are three main parameters that completely describe this model of transition: the transition onset location, the spot formation rate per unit span, and a spot growth parameter. Knowing these values, the transition length can be computed. These values are related to statistical properties of the transition region including the burst rate and average burst length, which are a function of intermittency.[10] These relationships for low-speed flow are described in detail in Ref. 10.

This type of transition model allows the computation of flow properties throughout transition.[11–13] For example, by combining the pressure fluctuations associated with wave packets and turbulent spots with this model of transition, the models can be extended to calculate transitional pressure fluctuations from fundamental physics. This type of model has already been developed for incompressible flow on a flat plate.[13] Some work to develop these models at high speeds has also been conducted.[14,15]

In order to develop similar models at high speeds and to improve prediction of hypersonic pressure fluctuations, experiments were conducted on a 7° sharp cone at zero angle of attack in the Sandia National Laboratories Hypersonic Wind Tunnel (HWT) at Mach 5, 8, and 14.[16] These measurements showed that the transitional boundary layer at high Mach numbers is complicated. There are large regions of second-mode instability waves intermixed with turbulence.[16,17] Traditional low speed intermittency computation methods only consider turbulent/non-turbulent regions.[8,9] However, for hypersonic flow, large regions of second-mode instability waves are observed in the transition region intermixed with turbulent regions. These waves include large surface pressure fluctuations which must be considered when developing appropriate

models of the transitional pressure field.

The simultaneous surface pressure measurements and schlieren images from Ref. 16 were used in the present work to develop methods of distinguishing second-mode instability waves from turbulence. Separate but complementary methods were developed for both the surface pressure measurements as well as for the schlieren videos. These were used to compute the intermittency, burst rate, and average burst length of both the instability waves and turbulent spots throughout transition. The development of these algorithms and initial results for several cases at Mach 5 and 8 are presented here. Work continues to refine and develop these algorithms and apply them to additional cases.

II. Experimental Setup

II.A. Sandia Hypersonic Wind Tunnel

The Sandia Hypersonic Wind Tunnel (HWT) is a conventional blowdown-to-vacuum facility. Interchangeable nozzle and heater sections allow the tunnel to be run at Mach 5, 8 or 14. Run times were typically 30 s. Mach 5 tests use air as the driver gas. HWT-5 has a P_0 range of 345–1380 kPa and a T_0 range of 330–890 K, giving a Re range of $3.3–26 \times 10^6/m$. Noise levels vary from 1–2% in this tunnel.[18] HWT-8 uses 689 MPa nitrogen supplied from a bottle farm. It has a P_0 range of 1720–6890 kPa, T_0 range of 500–890 K, and Re can be varied from $3.3–20 \times 10^6/m$. Noise levels vary from 3–5%.[18]

Freestream conditions in this tunnel are computed using the Beattie-Bridgeman model to account for real-gas effects. At the low freestream temperatures in these tunnels, a linear viscosity law is used. Edge conditions used for normalization of the data were computed using a Taylor-Maccoll solution for flow over the cone.

II.B. High-Speed Schlieren System

A high-speed schlieren system was developed to take images at a high frequency while also being able to resolve the detailed structure of the boundary-layer disturbances. Fig. 2 shows a simple schematic of the final system design. Figs. 3(a) and 3(b) show pictures of the setup.

The light source was a Flashpoint II 1220A Monolight which emits white light. This light has a flash energy rating of 600 Watt-seconds and a flash duration between 1–2 ms. The light could be fired every 2.5 seconds, allowing ten short movies to be captured during a typical run. The light from the source was passed through a slit to increase sensitivity and provide a more well-defined effective source. Two 101.6-mm diameter convex lenses with a 1-m focal length were then used to collimate the remaining light, pass it through the test section, and focus the light on a knife edge. The lenses were equally spaced on either side of the tunnel centerline. Most of the light was cutoff at the knife edge in order to increase the sensitivity of the schlieren system. The remaining light was then passed to a Phantom v12.1 digital camera. The slit, knife edge, and camera were all tilted 7° from horizontal to line up with the cone surface.

The Phantom camera was used for its high light sensitivity, fast imaging capabilities, and short exposure time. The camera has a fill factor of 56% and a 20 μm pixel size. The minimum exposure time of 285 ns was used for all images. The lens used with the camera was varied between a 85, 105, and 180-mm lens with f-stops of f/1.8, f/2.8, and f/3.5, respectively. The 180-mm lens was typically used at Mach 5 to give better resolution in the thin boundary layer. The 105-mm lens was mostly used for Mach 8 and 14; resolution was sacrificed in order to retain more light needed at the lower freestream densities at higher M. The exact resolution and framing rate was changed from run to run. Typical framing rates varied between 70–300 kHz. The array size varied between 1024×80 pixels and 512×32 pixels for these framing rates. Three to six hundred usable images were captured per movie; the exact number depended on the framing rate for a given run.

The schlieren images integrate through a curved boundary layer. The maximum azimuthal integration length at the middle of the schlieren viewing area was estimated by calculating the length of the circular segment at the radius of the cone R plus the boundary layer thickness δ, at a height R. At Mach 5 and $Re = 4.39 \times 10^6/m$, the boundary layer thickness is approximately 1.3 mm as determined optically from the schlieren images. This gives a maximum azimuthal integration length of approximately 17 times the boundary-layer thickness. At Mach 8 at a similar Re, the maximum azimuthal integration length is approximately 12 δ (δ is approximately 2.4 mm). This could affect the statistics computed from the schlieren images, since the integration area is wide compared to the boundary-layer thickness. However, the depth

of field of the camera lenses are much smaller. The depth of field was estimated to be on the order of 0.5 mm or less for the current setup. This would greatly reduce the integration effects since the depth of field is smaller than both the boundary layer thickness and the estimated azimuthal integration length.

Images were post-processed by applying a flat-field correction. The images were then contrast enhanced to emphasize the boundary-layer disturbances; the top 0.1% of the images was saturated. A gamma correction ($\gamma = 1.5$) was applied to nonlinearly weight the images towards darker values.

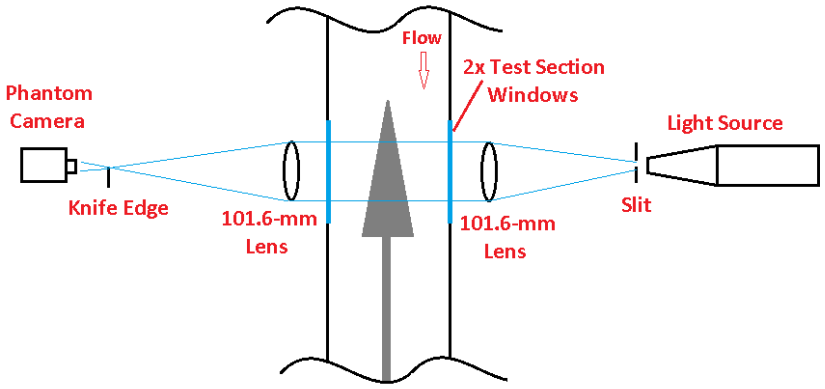

Figure 2. Schematic of the high-speed schlieren system developed for the Sandia Hypersonic Wind Tunnel.

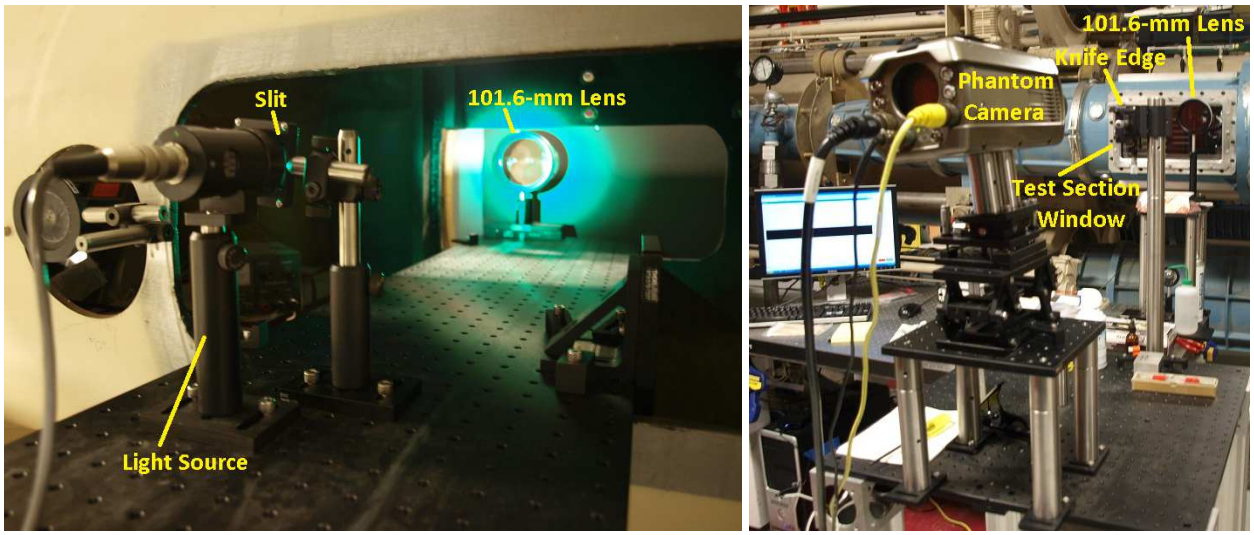

(a) (b)

Figure 3. High-speed schlieren system. The LED light source used for alignment is shown in place of the Flashpoint Monolight.

II.C. Model and Instrumentation

A 0.517-m-long 7° half-angle stainless-steel cone with a sharp nose (radius less than 0.05 mm) was used for this work (Fig. 4(a)). This cone has been used in previous experimental campaigns,[16,18–21] but the current analysis focuses on simultaneous schlieren and pressure measurements from Ref. 16. An axial array (Fig. 4(b)) with five PCB132 pressure sensors spaced 5.1 mm apart was used for pressure measurements. The fourth PCB132 sensor at x = 0.386 m was not working for these tests. There are additional Mic-062 Kulite pressure sensors in the axial array but those measurements are not discussed here. A downstream PCB132 pressure sensor was also located in a spanwise insert at x = 0.452 m. The schlieren viewing area was centered around the axial array (between x = 0.326 and 0.416 m) to allow simultaneous schlieren imaging and high-

frequency pressure measurements. Table 1 list the location of the pressure sensors and the schlieren viewing area.

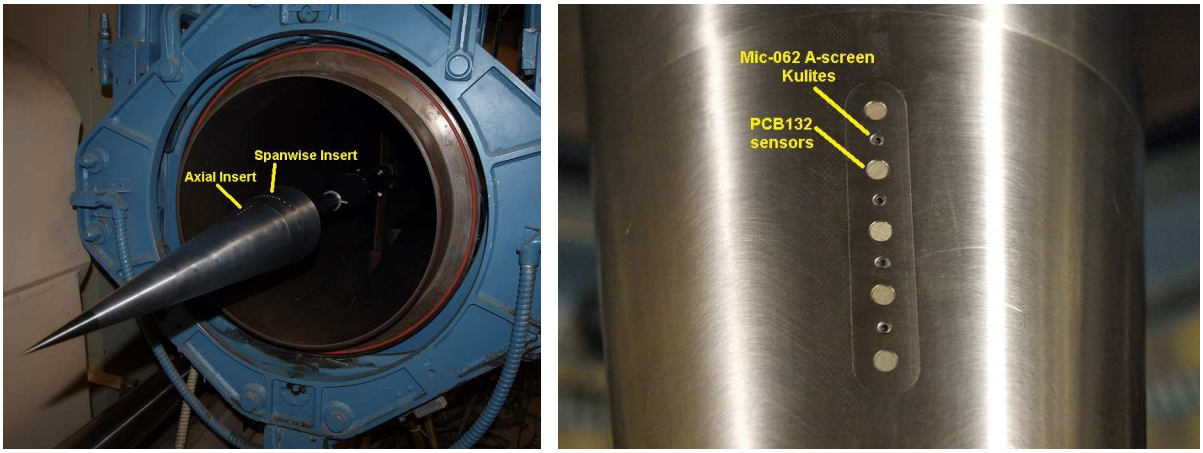

(a) (b)

Figure 4. Wind-tunnel model (a) Cone installed in Sandia Hypersonic Wind Tunnel; (b) Close-up view of axial insert showing closely spaced pressure instrumentation.

Table 1. Axial location of schlieren viewing area and pressure sensors on the 7° cone.

Location	Sensor	x (m)
Beginning of Schlieren Viewing Area		0.326
A1	PCB132	0.355
A3	PCB132	0.365
A5	PCB132	0.376
A7	PCB132	0.386
A9	PCB132	0.396
End of Schlieren Viewing Area		0.416
Spanwise Insert	PCB132	0.452

The growth and breakdown of the second-mode instability leading to transition can be studied with the PCB132 sensors. The sensor is a very high frequency piezoelectric time-of-arrival sensor. The resonant frequency is above 1 MHz; however, the sensor output is high-pass filtered at 11 kHz, per the manufacturer's specifications. Because the PCB132's can measure pressure fluctuations between 11 kHz and 1 MHz, they allow a study of instability breakdown to transition and are useful indicators of transition on the model. Also, the sensors have adequate frequency response to resolve the short duration of turbulent spots on the cone. However, the amplitude response of the sensors has not yet been accurately calibrated. In addition, the sensors have spatial resolution limitations. Second-mode waves have a wavelength of approximately twice the boundary-layer thickness (δ is about 1–3 mm for measurements on a typical cone model). The PCB132 diameter (3.18 mm) is larger than half of the instability wavelength on the cone. The actual sensitive area of the face is smaller, but its exact area is unknown. Some initial calibration work has been completed,[22,23] but more in-depth calibration is still needed. A shock tube has recently been built at Purdue for these purposes.[24]

II.D. Data Acquisition

The PCB132 sensors all run through a PCB 482A22 signal conditioner that provides constant-current excitation to the built-in sensor amplifier. It also decouples the AC signal from the DC bias voltage. The output from the signal conditioner is fed through a Krohn-Hite Model 3944 Filter with a 1.25 MHz low-pass anti-aliasing Bessel filter. This filter has four poles and offers 24 dB of attenuation per octave. The sampling frequency for the PCB132 sensors was 2.5 MHz. Pressure sensor data was acquired using a National Instruments PXI-1042 chassis with 14-bit PXI-6133 modules (10 MHz bandwidth). Ten 0.2-s segments of data

were acquired every 2.5 seconds during each run. These segments were triggered by a Stanford Research Systems DG645 Digital Delay Generator that also simultaneously triggered the light source and camera of the schlieren system.

III. Experimental Results

Methods to separate instability waves from turbulence were developed for both the surface pressure measurements and simultaneous schlieren videos. Consider first a transitional case at Mach 5. Figure 5 shows a typical schlieren sequence at an intermediate Re of $9.75 \times 10^6/m$. The red arrows mark the location of four PCB132 sensors beneath the viewing area at x = 0.355, 0.365, 0.376, and 0.396 m. In this case, a low-frequency disturbance is seen convecting within a smooth, laminar boundary layer (Figs. 5(a) – 5(b)). Higher frequency periodic waves develop on top of this low-frequency disturbance (Figs. 5(c) – 5(d)). The disturbance then breaks down into a turbulent spot that continues to convect and grow downstream (Figs. 5(e) – 5(j)). Stability analyses show that the low-frequency disturbance is likely a first-mode wave, while the higher frequency periodic disturbances are second-mode instability waves.[16]

Fig. 6 shows simultaneous pressure traces and the corresponding power spectral densities (PSD's) for this case. The bounding times of the schlieren sequence are shown with vertical black lines. The traces are offset from each other proportional to their axial location on the cone to show the growth and convection of boundary-layer disturbances. PSD's were computed from these 200 μs pressure traces using a Blackman window. Because only a single time trace is used for the computation, the plots are noisy (there is no averaging). Also, because of the short time traces used, the resolution of the spectra is only 5 kHz. However, the spectra can still indicate the frequency of the boundary-layer disturbances.

The pressure trace from the first sensor at x = 0.355 m shows large high-frequency waves passing by, in agreement with the schlieren images. There is also a lower frequency oscillation in the pressure traces near 30 kHz, which occurs for unknown reasons. The corresponding PSD shows a peak between 200 and 400 kHz, at a range expected for the second-mode instability. The low-frequency first-mode disturbance is not observed in the surface pressure fluctuations, but may be obscured by freestream tunnel noise which is largest at low frequencies. The pressure traces from the last three sensors between x = 0.365 and 0.396 m show a turbulent disturbance passing by, also in agreement with the schlieren images. The corresponding spectra indicate more broadband frequencies as expected for a turbulent disturbance.

It is desired to compute the transition statistics directly from the surface pressure measurements. A typical low-speed method to characterize boundary-layer intermittency is given by Ching and Lagraff.[25] This method is based on a generalized procedure by Hedley and Keffer that differentiates turbulent and non-turbulent flow.[26] The procedure takes an intermittent signal and first sensitizes it by using a detector function. This detector function typically differentiates and squares the signal in order to emphasize the high-frequency components. This detector function is then smoothed by averaging over a short time interval. This removes any zeros that are part of the turbulence and would otherwise signal the end of a turbulent region. This step creates what is called a criterion function. The final step is to set a threshold level. Above the threshold, the flow is considered turbulent and below it, the flow is considered laminar. By applying this threshold, an indicator function consisting of ones (for turbulent flow) and zeros (for laminar flow) is created. Each of these steps is somewhat arbitrary. Different detector functions, different amounts of smoothing, and different threshold levels can be chosen, and these must be set based on the data. Ching and LaGraff used one such method to find the leading and trailing edges of turbulent spots at low speeds.[25] This technique has been used previously to calculate boundary-layer intermittency in high-speed flow.[15,17] The method was able to distinguish disturbances from laminar flow, but could not separate instability waves from turbulence.

An improved method to identify the disturbances and also distinguish instabilities from turbulence was developed in the present work using the wavelet transform. This technique shows the frequency content of the disturbances as a function of time, and has been used in other unsteady applications such as wake transition, meteorological studies, and cavity flows.[27–29] The transform provides good time resolution for identifying intermittent disturbances. However, it has poor frequency resolution compared to alternate joint time-frequency methods such as the short-time-Fourier transform.

Fig. 7 shows an example of the wavelet transform computed for the pressure traces in Fig. 6(a). The transform was computed using Matlab software from Ref. 28. A Morelet mother wavelet was used. The evolution of the frequency content of the disturbance can be clearly seen with downstream distance. At x = 0.355 m (Fig. 7(a)), the disturbance is still an instability wave packet. High levels of frequency content are

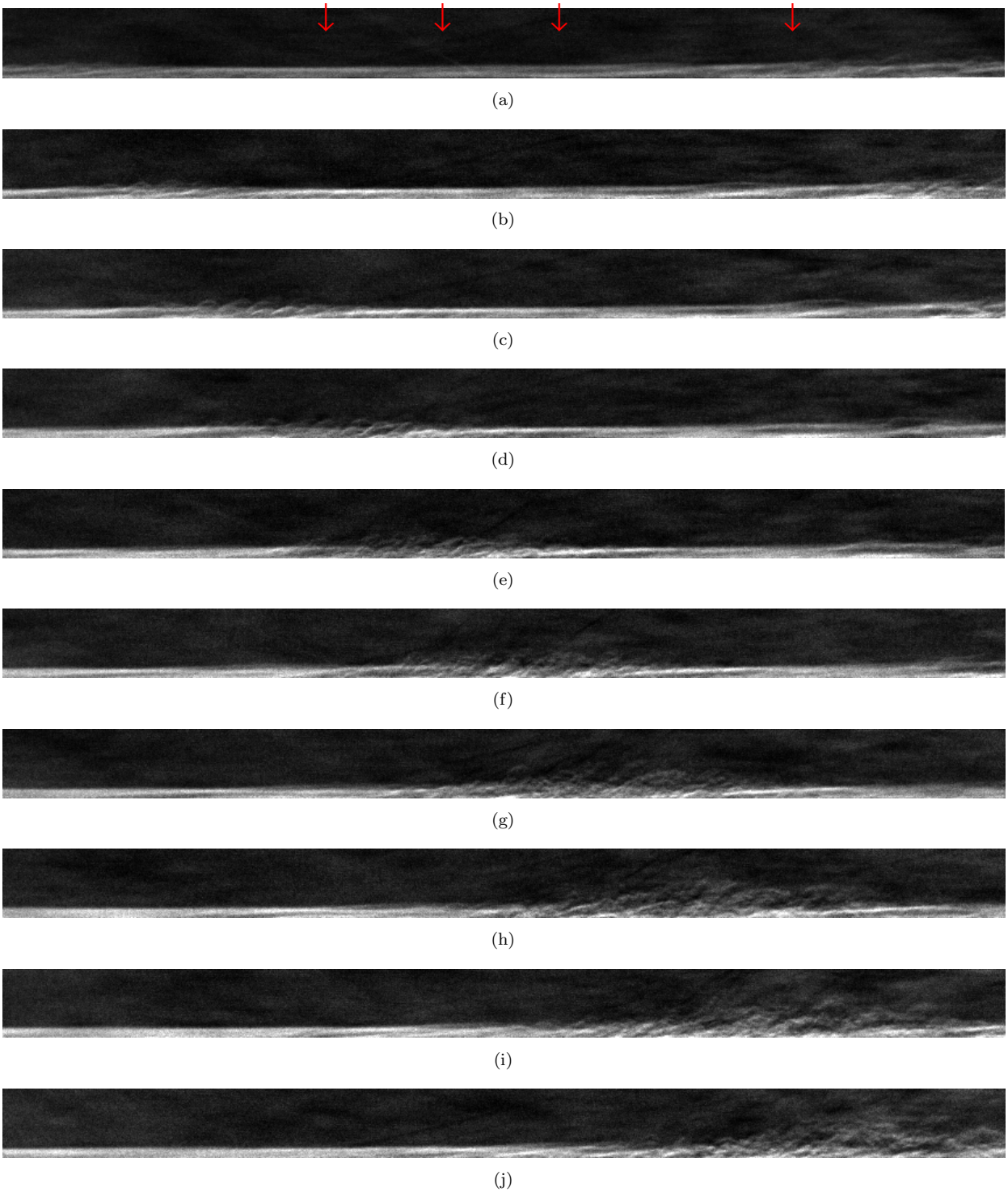

Figure 5. Schlieren images showing intermittent disturbances within mostly laminar flow. Red arrows mark the location of surface mounted PCB132 pressure sensors. HWT-5, $\Delta t = 11\mu s$**,** 1024×64 **pixel array size,** $Re = 9.75 \times 10^6/m$**,** $M = 4.96$**,** $P_0 = 650.3\ kPa$**,** $T_0 = 446.6\ K$**.**

concentrated between 200-600 kHz, with a peak near 350 kHz. There is also a low frequency band near 30 kHz that remains fairly continuous in time. This is the low-frequency oscillation observed in the time traces whose origin is unknown.

Further downstream (Figs. 7(b)-7(d)), the wave packet breaks down into a turbulent spot. High-frequency

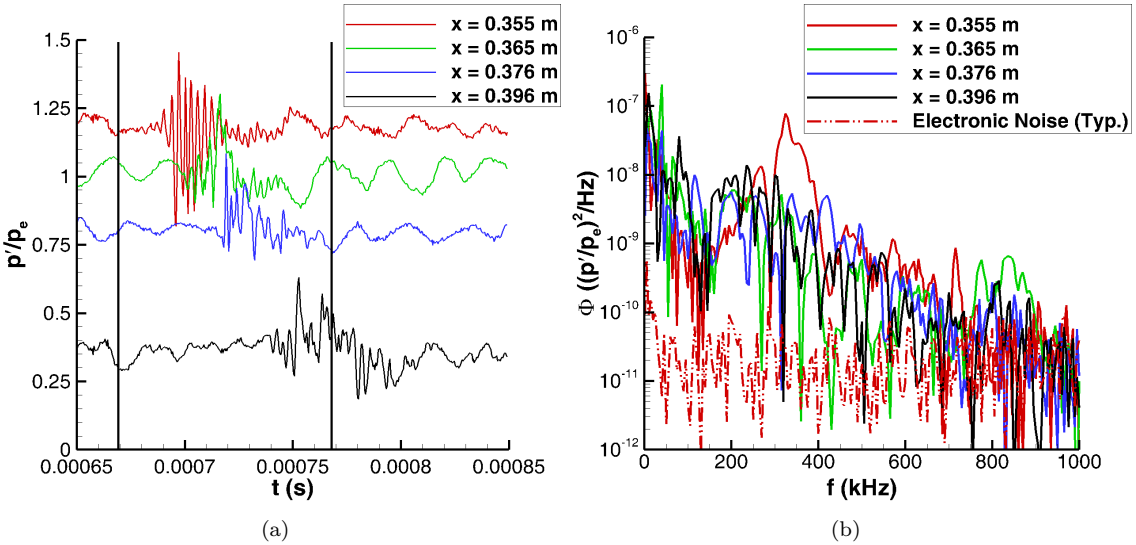

(a) (b)

Figure 6. Simultaneous pressure measurements, HWT-5, $Re = 9.75 \times 10^6/m$ (a) Pressure traces, each trace is vertically offset proportional to x. Vertical black lines mark the time interval of the corresponding schlieren images; (b) Power-spectral densities.

content is still observed above 200 kHz, though at a reduced level. The peak of the higher frequencies shifts downward to near 200 kHz. This region of high-frequency content also spreads in time as the disturbance grows. A low-frequency portion of the spectra also develops between 50–150 kHz. This low-frequency region grows in amplitude and time with downstream distance as the disturbance grows.

The wavelet transform of measurements from a downstream sensor at x = 0.452 m is also shown in Fig. 7(e). By this location, the majority of the time trace is turbulent. Regions of high and low frequencies are observed throughout the time interval. The convecting and growing turbulent spot observed in the upstream sensors is seen, along with additional regions of turbulence. These additional regions may have spread from other disturbances present in the spanwise direction.

A threshold criteria based on different frequency ranges in the transform can be used to separate the second-mode waves and turbulence. It is difficult to distinguish large, nonlinear second-mode waves from turbulence in the high-frequency range of the wavelet transform, since those high frequencies are common to both. Instead, the low frequency range between 50 and 150 kHz can be used. A magnitude threshold criteria is first applied over that region to determine when the signal is turbulent. For Mach 5, an amplitude threshold on the wavelet transform of 190 was used at $Re = 9.75 \times 10^6/m$ and was decreased to 95 by $Re = 15.4 \times 10^6/m$. If the signal is not identified as turbulent, then a separate magnitude threshold criteria on the results between 200 and 400 kHz are used to identify regions of instability waves. The high frequency threshold was set to 75 at $Re = 9.75 \times 10^6/m$ and decreased to 38 by $Re = 15.4 \times 10^6/m$. The low-frequency band threshold was applied first and had priority over the high-frequency threshold. This is because the high-frequency range is present for both instability waves and turbulence. These thresholds were set based on visual comparisons to the time traces. However, a lot of work remains to refine the techniques, apply them to additional cases, and quantify the sensitivity of the results to the chosen thresholds.

The results of applying this two-step technique for this case are shown in Fig. 8. Indicator signals with elevated dotted lines identifying turbulent regions and elevated dashed lines indicating areas of second-mode waves are shown superimposed on the pressure traces. Periodic components corresponding to the instability waves are captured, while more turbulent regions are separately identified. The method is also able to identify regions of waves at the leading and trailing edges of turbulent spots (for example, the disturbance seen at x = 0.365 and 0.376 m in Fig. 8), as was often observed in Ref. 17.

An analogous procedure to distinguish second-mode waves from turbulence was developed for the schlieren images. A 'Canny' edge detection method was first used to find edges in the schlieren images. This method finds the local maxima of the gradient of the images. The gradient is calculated using the derivative of a Gaussian filter. A dual threshold is used to detect both strong and weak edges in the images, but weak edges are maintained only if they are connected to strong edges. This dual threshold helps to distinguish weak edges from background noise in the images. Fig. 9 shows typical images of second-mode waves and turbulent

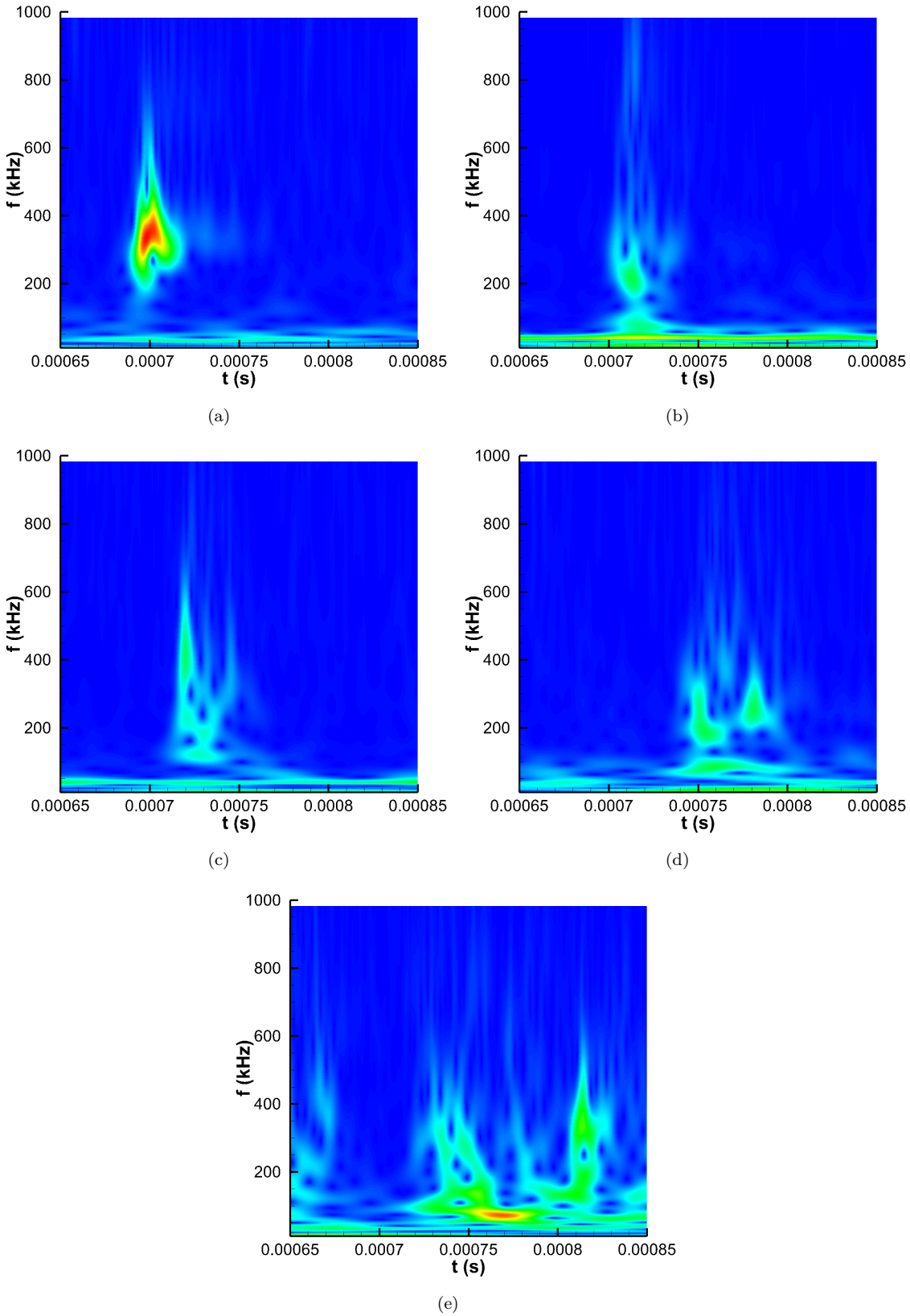

Figure 7. Wavelet transform of pressure measurements, HWT-5, $Re = 9.75 \times 10^6/m$ **(a) x = 0.355 m; (b) x = 0.365 m; (c) x = 0.376 m; (d) x = 0.396 m; (e) x = 0.452 m.**

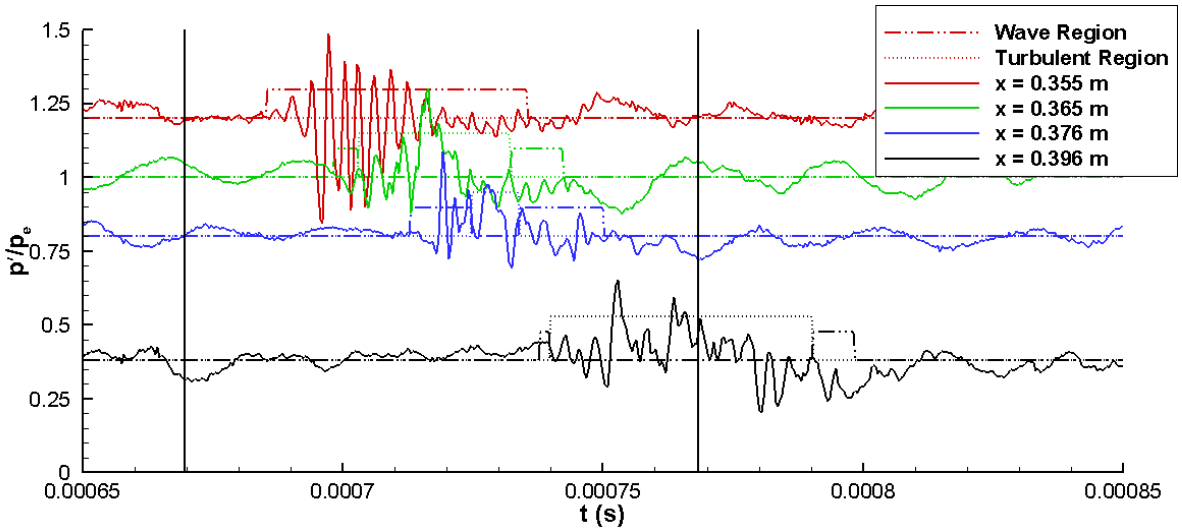

(a)

Figure 8. Wavelet transform thresholds applied to pressure measurements to distinguish turbulence and second-mode waves, HWT-5, $Re = 9.75 \times 10^6/m$. Elevated indicator signals mark regions of instability waves and turbulent spots.

spots with and without edges marked in red by this algorithm. The maximum y location of the edges was then found at each horizontal position. Local averages of the maximum edge locations were computed across the image (the length of the average was two times the laminar δ). These averages were then compared to the laminar boundary layer height δ. Values larger than the laminar δ were initially marked as turbulent (equal to 1), while those equal or less than the boundary-layer height were initially marked as laminar (equal to 0).

Second-mode waves are harder to distinguish in the schlieren images. A method based on the boundary-layer thickness does not work to pick out the waves, since the average boundary-layer height across regions of waves is near the laminar δ, but often above it. Instead, a correlation technique was used. Segments of the image (with a height of 1.5 and a length of 2 times the laminar δ, respectively) were cross-correlated with a longer region with a length of 6 δ to identify any periodic components. Segments with peaks in the correlation at the expected second-mode wave frequency range were identified as instability waves. This step supersedes the first step which initially marks the regions as laminar or turbulent.

This technique was applied to all images obtained during a schlieren video to obtain intermittency curves along the schlieren viewing area. Intermittency results from both the pressure measurements and simultaneous schlieren images at $Re = 9.75 \times 10^6/m$ are shown in Fig. 10(a). There is reasonable agreement between the two techniques; both show similar trends throughout the transition region. In this case, the intermittency of the second-mode waves is near 0.2 and fairly constant if slightly decreasing with downstream distance. The turbulent intermittency is increasing from near zero to over 0.8 with downstream distance. Also, the shape of the turbulent spot intermittency curves follows the expected error function shape seen in the literature.[8–10] The overall disturbance intermittency (sum of the instability and turbulent intermittencies) is also increasing with downstream distance but does not reach one. Because the intermittency of the instability waves remains low, there is not a large difference between the turbulent intermittency and the overall disturbance intermittency.

Results at a higher Re of $11.8 \times 10^6/m$ are shown in Fig. 10(b). Transition begins further upstream in this case, though the overall trends are similar to $Re = 9.75 \times 10^6/m$. The wave packet intermittency begins near 0.1 but then decreases towards zero as the turbulent intermittency increases from zero to near one. The overall disturbance intermittency is high in this case and approaches one. At the highest Re of $15.4 \times 10^6/m$ (Fig. 10(c)), the boundary layer is mostly turbulent. Some regions of second-mode waves are observed at the beginning of the schlieren viewing area, but the number of waves quickly decreases as fully turbulent flow is reached downstream. Again, the turbulent intermittency and overall disturbance intermittency are similar because the intermittency of second-mode instability remains small. The overall transitional behavior is similar to low-speed results. The turbulent burst intermittency curve follows the expected error-function shape seen in the literature, and isolated disturbances are observed surrounded by an otherwise smooth,

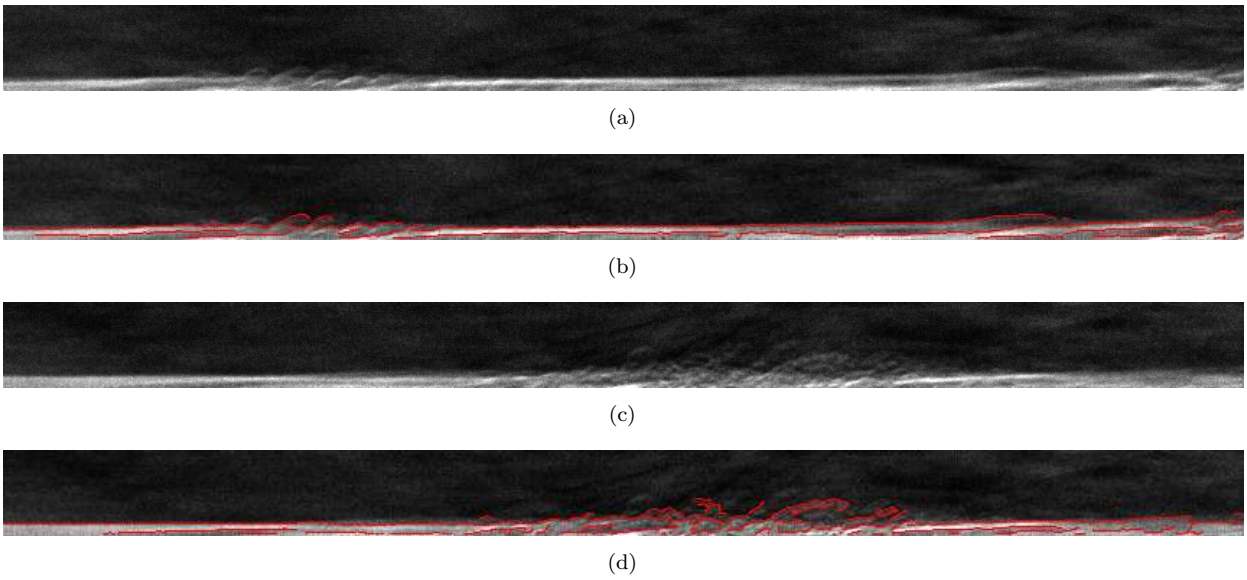

Figure 9. Edge detection in schlieren images, HWT-5, $Re = 9.75 \times 10^6/m$ (a) Typical wave packet; (b) Packet with edges marked by the 'Canny' algorithm; (c) Typical turbulent spot; (d) Spot with edges marked by the 'Canny' algorithm.

laminar boundary layer.[8–10] However, the presence of the instability waves is a significant difference from low-speed flow and becomes more important as the Mach number increases.

The burst rate and average burst length were also computed from the pressure measurements. These computations required applying an image close-open filter to the indicator signals to remove false triggers at the edges of the disturbances. These false triggers cause burst rates to be biased high and average burst lengths to be biased low if not removed. This filter uses two standard functions in Matlab ('imopen' followed by 'imclose') and was applied in 1D to the pressure measurements. The filtering performs a series of dilation and erosion operations on the data, and was set so that disturbances smaller than the period of a second-mode wave were removed.

Figs. 11 and 12 show the burst rate and average burst length at Mach 5 corresponding to the intermittency computations in Fig. 10. At the lowest Re of $9.75 \times 10^6/m$ (Figs. 11(a) and 12(a)), the burst rate of the instability waves, turbulent spots, and overall disturbances initially increases with downstream distance. This occurs at the same time that the intermittency of the turbulent bursts and overall disturbance intermittency is increasing. The overall disturbance rates are not merely the sum of the instability and turbulent spot burst rates because the two events often run together and form part of a single disturbance. The average burst length of the turbulent bursts and overall disturbances also increases as turbulent flow begins to dominate the boundary layer. This causes the average instability wave length and burst rate to decrease.

At an intermediate Re of $11.8 \times 10^6/m$ (Figs. 11(b) and 12(b)), the burst rates are highest near x = 0.360 m, where both the turbulent and overall disturbance intermittency are near 0.5. The instability intermittency remains at a lower level because the average length of the instability waves is much shorter. These packets are often attached to the ends of the turbulent regions. The burst rate decreases with downstream distance for the wave packets, turbulent spots, and overall disturbances as regions of these merge together. The average instability wave packet length remains small and fairly constant over this region. However, the average length of the turbulent spots and overall disturbances grows. By x = 0.396 m, the disturbance and turbulent lengths are off scale because the flow is mostly turbulent.

At the highest Re of $15.4 \times 10^6/m$ (Figs. 11(c) and 12(c)), the burst rate is low along the cone. Some alternating wave packets and turbulent spots are observed at x = 0.365 and 0.376 m, but this may disappear with refined threshold levels since the flow is predominately turbulent over the schlieren viewing area. The average burst length results for this case shows that turbulent spots are very long. Some brief periods of second-mode instabilities are observed, but only at a small rate. The disturbance burst rate is zero in all cases because the entire region of flow is occupied by either instability waves or turbulence. This also means that the disturbance length is very long.

The behavior of the turbulent spot burst rate and average spot length is qualitatively similar to low-

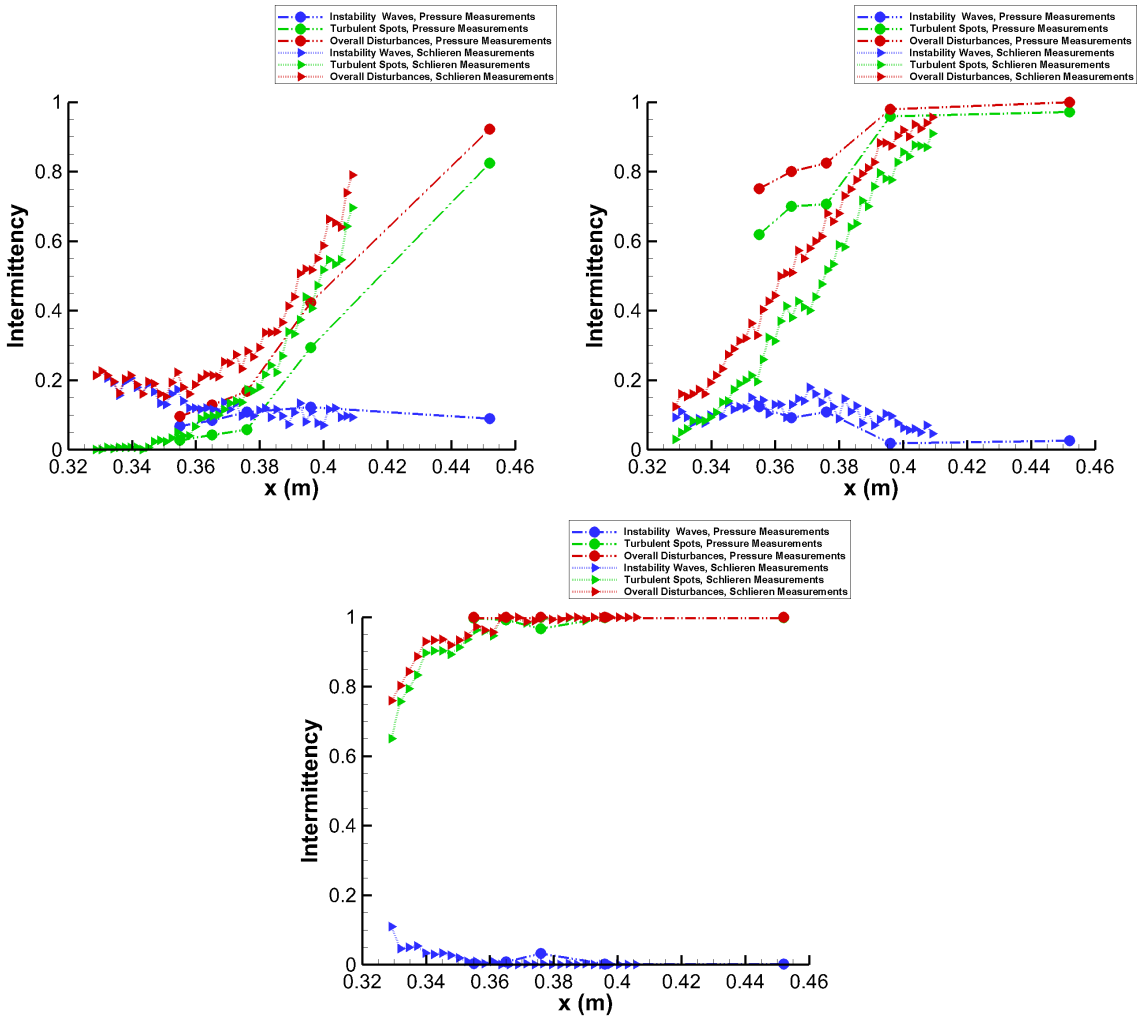

Figure 10. Intermittency along cone computed using the wavelet transform and schlieren techniques, HWT-5 (a) $Re = 9.75 \times 10^6/m$ **(b)** $Re = 11.8 \times 10^6/m$ **(c)** $Re = 15.4 \times 10^6/m$**.**

speed flow.[10] The burst rate peaks midway through transition and the average length of the turbulent spots increases. However, the presence of instability waves is an added complexity at Mach 5. These waves become more important to the transition behavior as Mach number is increased.[16]

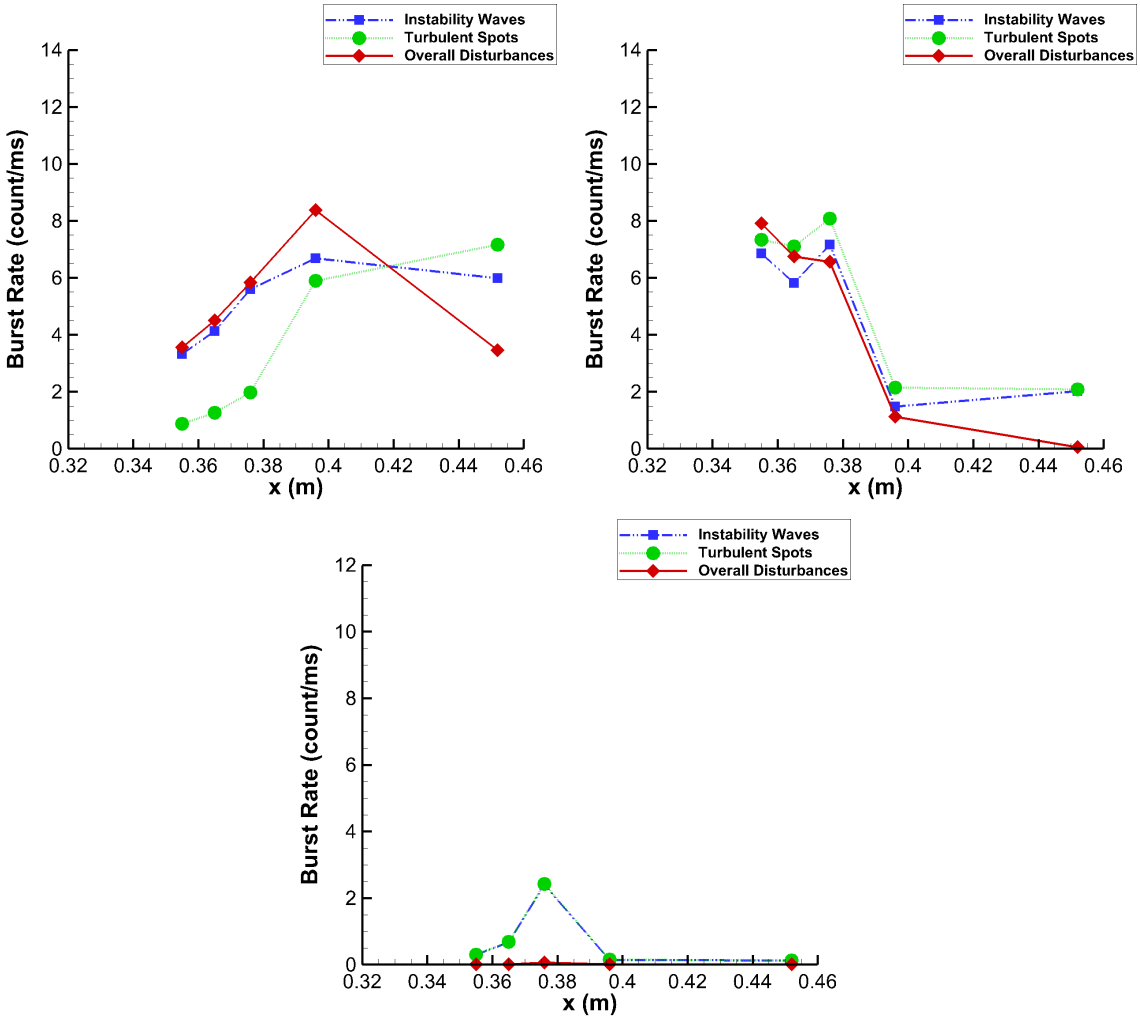

Figure 11. Burst rate along cone computed from pressure measurements, HWT-5 (a) $Re = 9.75 \times 10^6/m$; **(b)** $Re = 11.8 \times 10^6/m$; **(c)** $Re = 15.4 \times 10^6/m$.

The same techniques were also applied to Mach 8 data. At this higher Mach number, the character of the boundary layer is different. At Mach 5, isolated wave packets and spots were found within a laminar boundary layer. At Mach 8, the flow is dominated by second-mode waves before turbulent spots begin to appear within them. There are essentially no laminar regions when the spots form.[16] A typical schlieren sequence demonstrating this behavior is shown in Fig. 13 at a Re of $9.74 \times 10^6/m$. At this condition, larger patches of turbulent flow have developed, but these are still surrounded by second-mode instability waves. The simultaneous pressure traces appear mostly turbulent, with only small regions of periodic second-mode waves (Fig. 14(a)). The corresponding PSD's show broadband frequencies indicating mostly turbulent flow, though there are still remnants of second-mode peaks in the spectra near 200 kHz (Fig. 14(b)).

The same wavelet transform technique was applied to the pressure measurements at Mach 8 to separate instability waves and turbulence. Fig. 15 shows an example of the wavelet transform computed for the pressure traces in Fig. 14(a). The wavelet transform again shows two regions that can be used to separate periodic waves from turbulence. In this case, a low-frequency band between 50 and 100 kHz was used to identify turbulent regions, and a higher frequency band between 175 and 350 kHz was used to identify second-mode waves. The thresholds used at Mach 8 were different that at Mach 5. The low-frequency threshold was 150 at $Re = 7.1 \times 10^6/m$ and decreased to 93 at $Re = 9.74 \times 10^6/m$, while the high-frequency threshold was set at 27. These values were again chosen to give reasonable agreement with the data. In

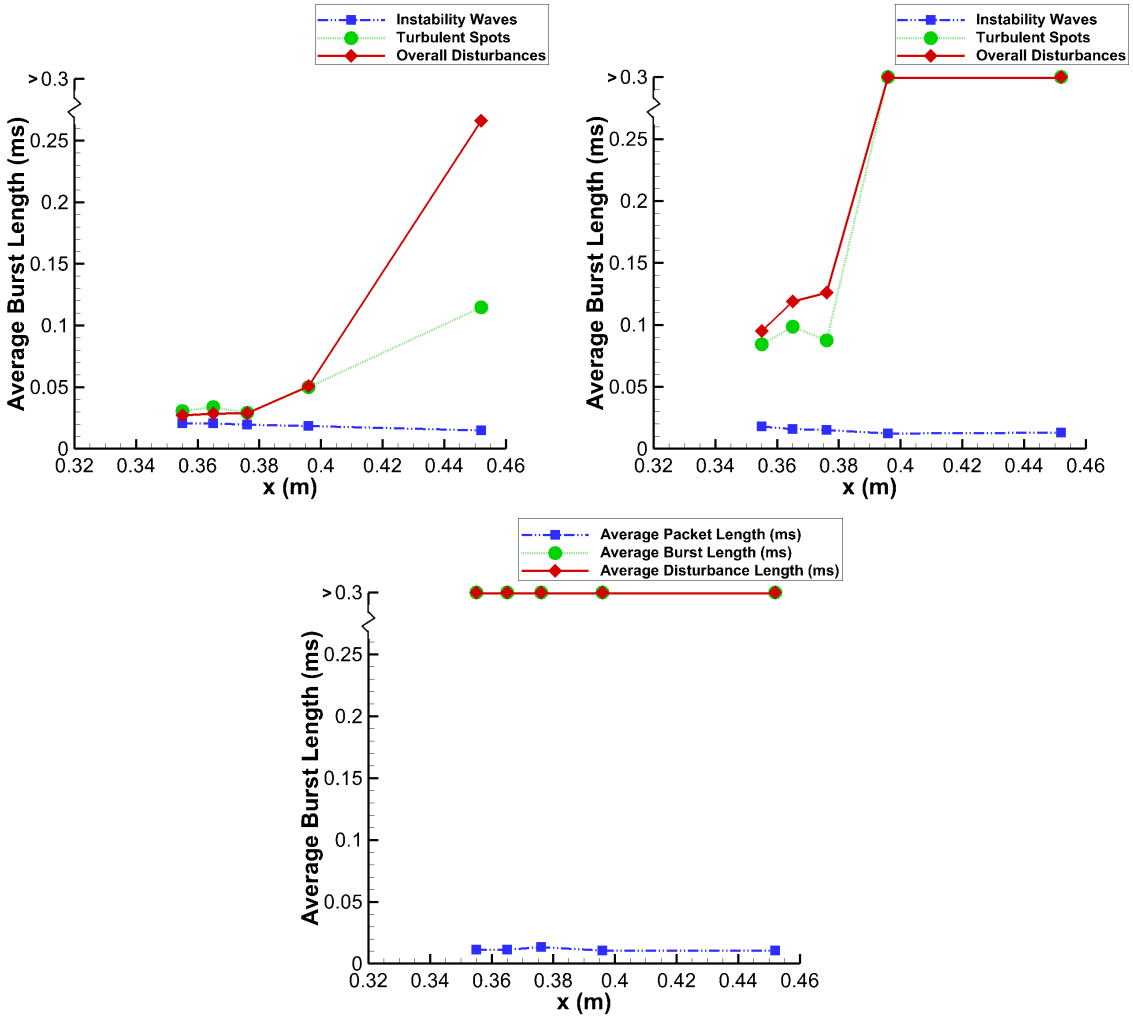

Figure 12. Average burst length along cone computed from pressure measurements, HWT-5 (a) $Re = 9.75 \times 10^6/m$**; (b)** $Re = 11.8 \times 10^6/m$**; (c)** $Re = 15.4 \times 10^6/m$**.**

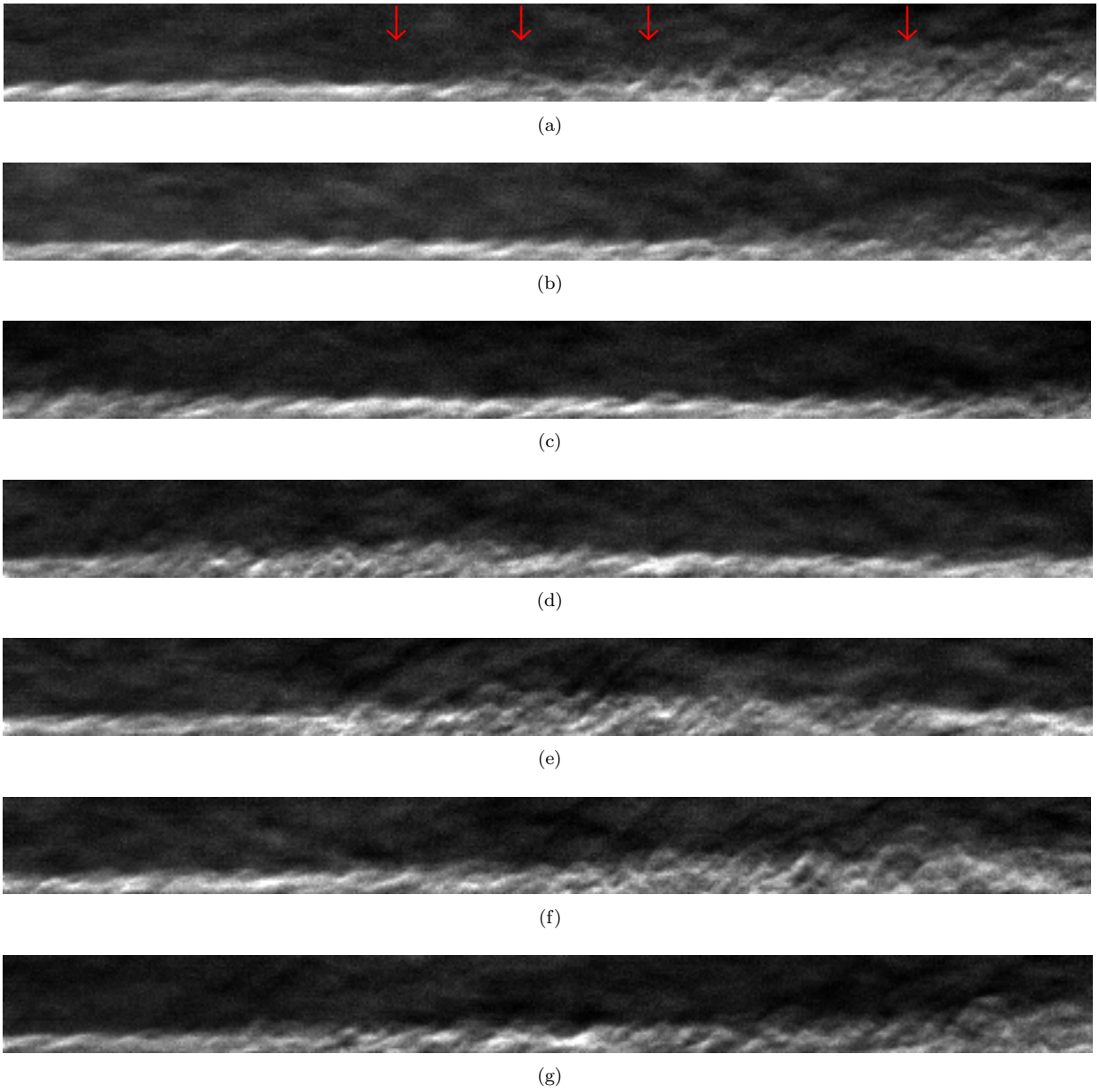

(a)

(b)

(c)

(d)

(e)

(f)

(g)

Figure 13. Schlieren images showing intermittent turbulent disturbances surrounded by second-mode instability waves. Red arrows mark the location of surface mounted PCB132 pressure sensors. HWT-8, $\Delta t = 5\mu s$, 512×48 pixel array size, $Re = 9.74 \times 10^6/m$, $M = 7.87$, $P_0 = 3338\ kPa$, $T_0 = 611\ K$. Every fifth image of the schlieren movie is shown.

the future, these thresholds will be refined and a sensitivity analysis will be done to quantify the effect the thresholds have on the results.

The result of applying the wavelet transform technique to the pressure measurements is shown in Fig. 16. Again, different regions corresponding to either turbulence or second-mode waves are marked. In this case, the flow is mostly turbulent, but regions of periodic waves are identified as they pass by the sensors.

The same schlieren technique used at Mach 5 to separate turbulence and waves was also used at Mach 8. However, the flow in the schlieren viewing area at Mach 8 was dominated by second-mode waves. The boundary-layer thickness used to mark turbulent regions for the algorithm at Mach 8 was determined by averaging all images during a run. This averaged through the second-mode waves and gave a smooth estimate of the non-turbulent boundary layer thickness. Even though this estimate will be higher than an undisturbed laminar boundary layer because of the presence of waves, it can still able to be used to determine what portions of the flow are turbulent. Regions of instability waves were then marked by the

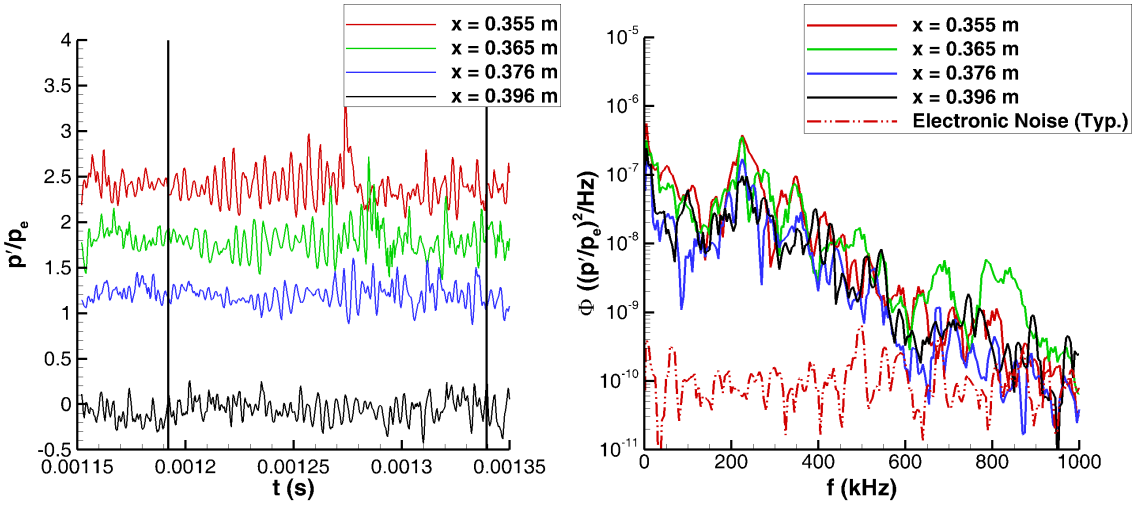

(a) (b)

Figure 14. Simultaneous pressure measurements, HWT-8, $Re = 9.74 \times 10^6/m$, $M = 7.87$, $P_0 = 3338\ kPa$, $T_0 = 611\ K$ (a) Pressure traces, each trace is vertically offset proportional to x. Vertical black lines mark the time of the corresponding schlieren images; (b) Power-spectral densities.

same correlation technique used at Mach 5.

The different boundary-layer character at Mach 8 is captured by the intermittency results (Fig. 17(a)). Once again, there is reasonable agreement between the schlieren and pressure measurements. As opposed to Mach 5, the intermittency of the second-mode waves reaches near one before turbulent spots appear. This is especially clear in the pressure measurements, which are more sensitive to small second-mode waves. Once turbulent spots appear, the intermittency of the wave packets decreases; however, the combined intermittency of the disturbances remains near one. A similar behavior is also seen at a higher Re of $9.74 \times 10^6/m$ (Fig. 17(b)). The overall disturbance intermittency remains near one through the transitional region; however, the instability intermittency is actually decreasing towards zero as the turbulence intermittency is increasing towards one. The turbulent intermittency curve at Mach 8 still follows an error-function shape, similar to low-speed flow,[8–10] even though the spots are born within flow dominated by instability waves.

The burst rate and average burst length were also computed from the Mach-8 pressure measurements. Results at varying Re are shown in Figs. 18 and 19. At $Re = 7.1 \times 10^6/m$ (Figs. 18(a) and 19(a)), the instability and turbulent spot burst rates are essentially identical. This happens because the overall disturbance intermittency is one. The flow is either a second-mode wave or a turbulent region and alternates between the two states. The burst rate increases with downstream distance as more regions of turbulence develop within the instability waves. The average length of the instability regions is falling as turbulent spots develop within them. The average length of the turbulent spots, however, is still small because the turbulent spot intermittency is low, and the spots are just beginning to form within the instability waves. The average disturbance length, however, remains very long because the disturbance intermittency is one.

At the highest Re of $9.74 \times 10^6/m$ (Figs. 18(b) and 19(b)), the flow is mostly turbulent. This causes the burst rate of the instabilities and turbulent spots to decrease along the cone as turbulence dominates. The burst rate is again identical for the instabilities and turbulent spots because the overall disturbance intermittency is one. This also means that the overall disturbance burst rate is zero. The average burst length of the turbulent spots is initially small when the turbulent spot intermittency is low, and the spots are just beginning to form. The average length of the spots then increases with downstream distance as the turbulent intermittency rises. The average instability wave length remains small through this region. However, the overall disturbance lengths are long because the flow is alternating between growing turbulent regions and short regions of wave packets interspersed in the flow.

At Mach 8, the character of the boundary layer changes as do the accompanying transition statistics. The overall disturbance and turbulent intermittencies are quite different throughout the transition region. This is because a large part of the flow is dominated by instabilities. The burst rate of the instabilities and turbulent spots is the same through transition because the flow alternates between the two states. However, the average length of the instabilities decreases while the turbulent spots grow in length.

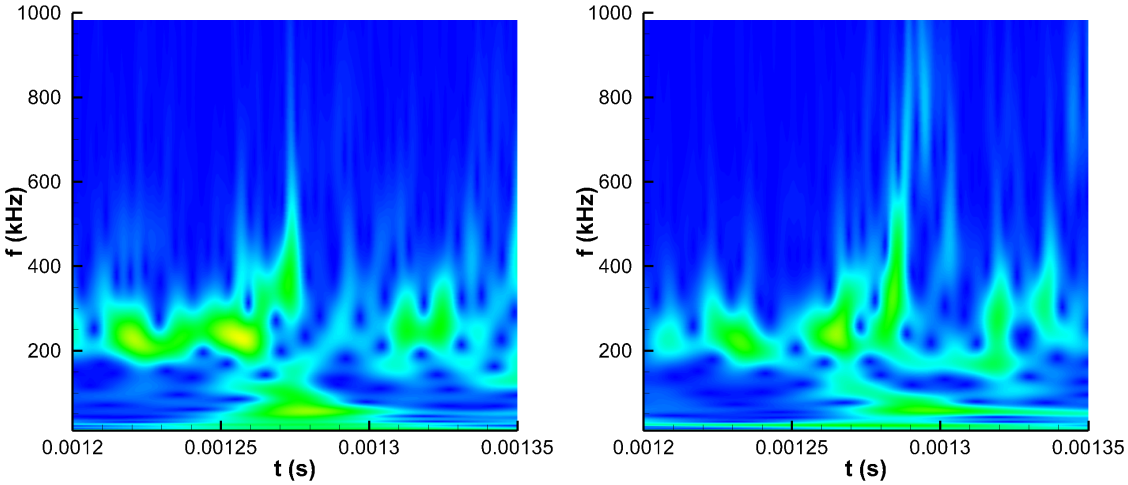

(a)

(b)

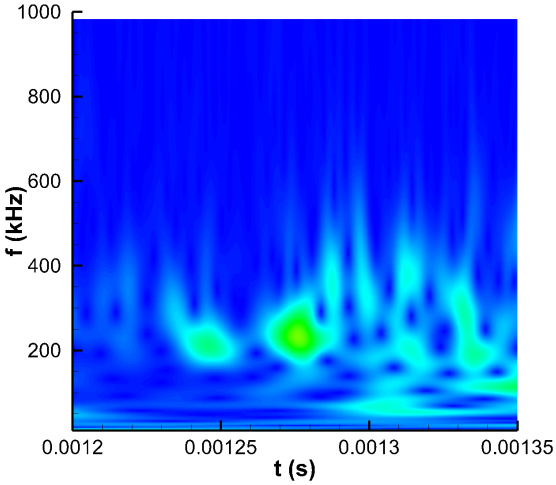

(c)

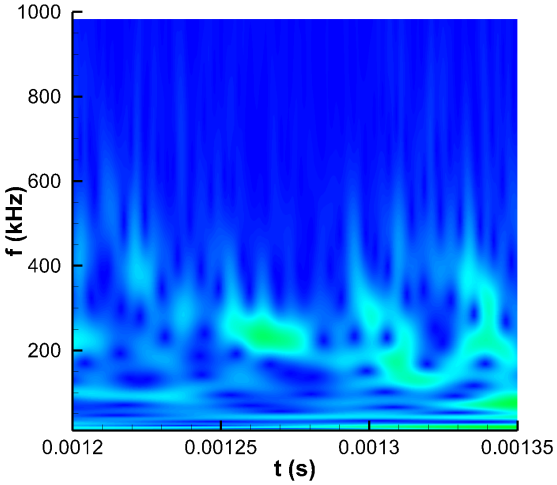

(d)

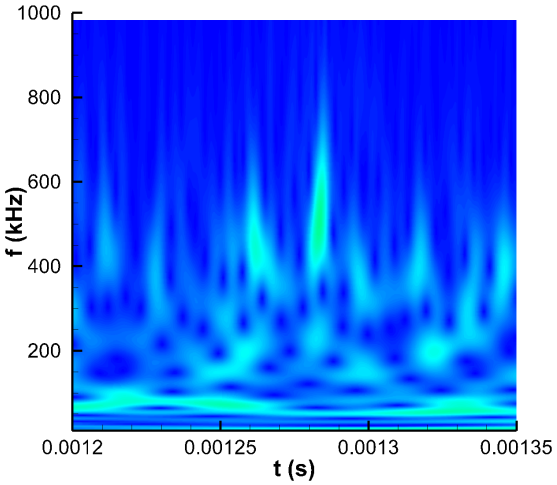

(e)

Figure 15. Wavelet transform of pressure measurements, HWT-8, $Re = 9.74 \times 10^6/m$ **(a) x = 0.355 m; (b) x = 0.365 m; (c) x = 0.376 m; (d) x = 0.396 m; (e) x = 0.452 m.**

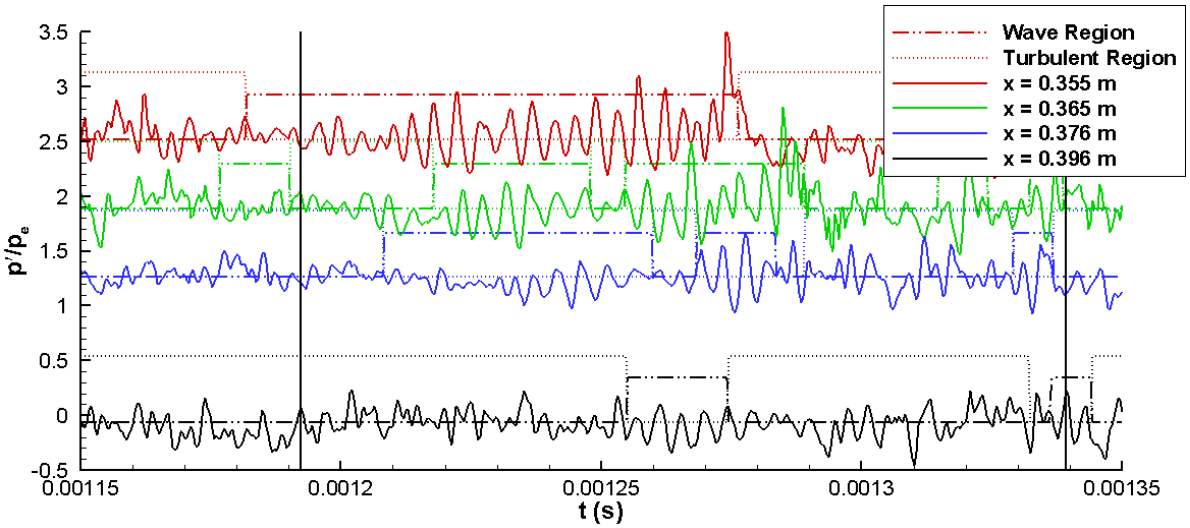

(a)

Figure 16. Wavelet transform thresholds applied to pressure measurements to distinguish turbulence and second-mode waves, HWT-8, $Re = 9.74 \times 10^6/m$**. Elevated indicator signals mark regions of instability waves and turbulent spots.**

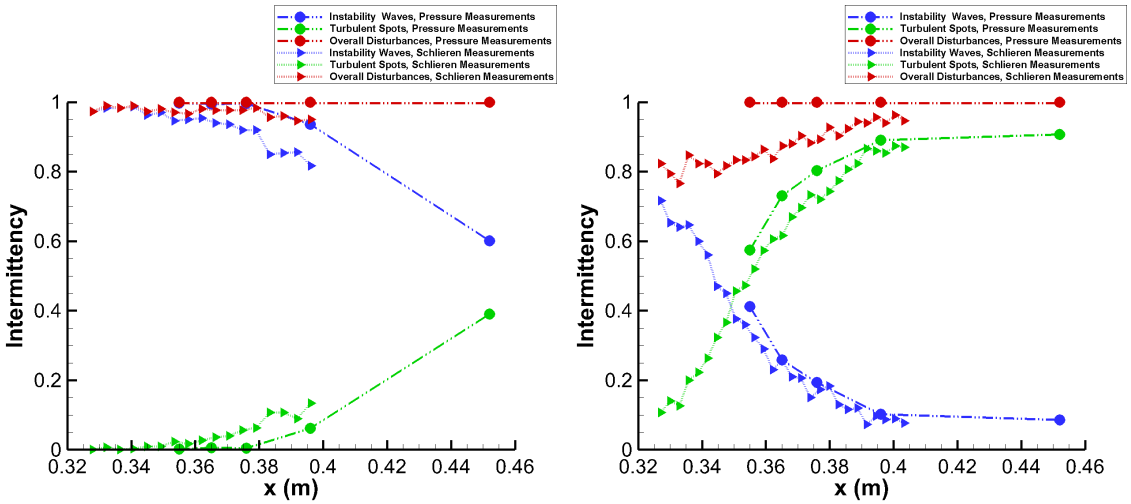

(a) (b)

Figure 17. Intermittency curves computed using the wavelet transform and schlieren techniques, HWT-8 (a) $Re = 7.1 \times 10^6/m$**; (b)** $Re = 9.74 \times 10^6/m$**.**

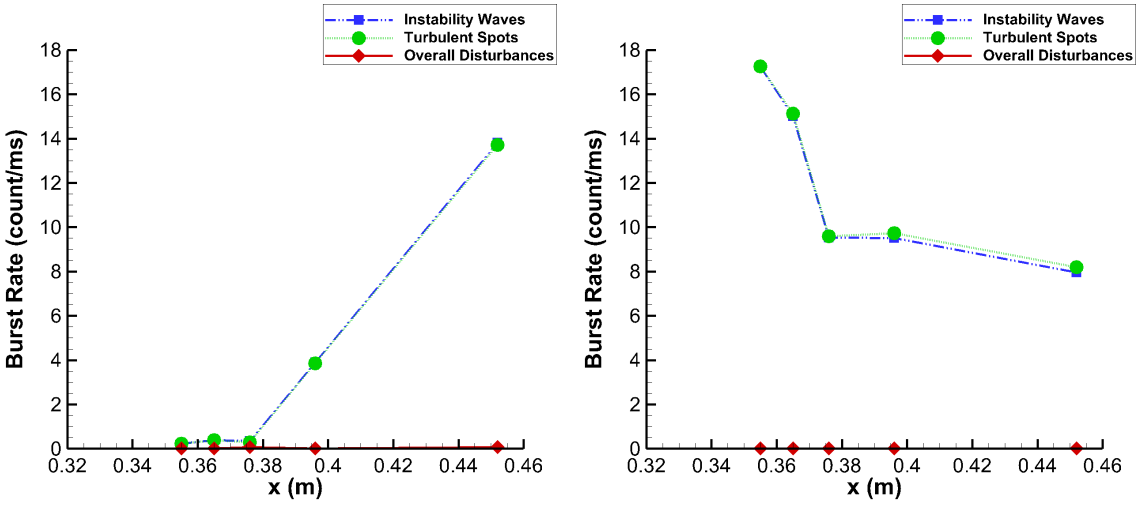

Figure 18. Burst rate along cone computed from pressure measurements, HWT-8 (a) $Re = 7.1 \times 10^6/m$**; (b)** $Re = 9.74 \times 10^6/m$**.**

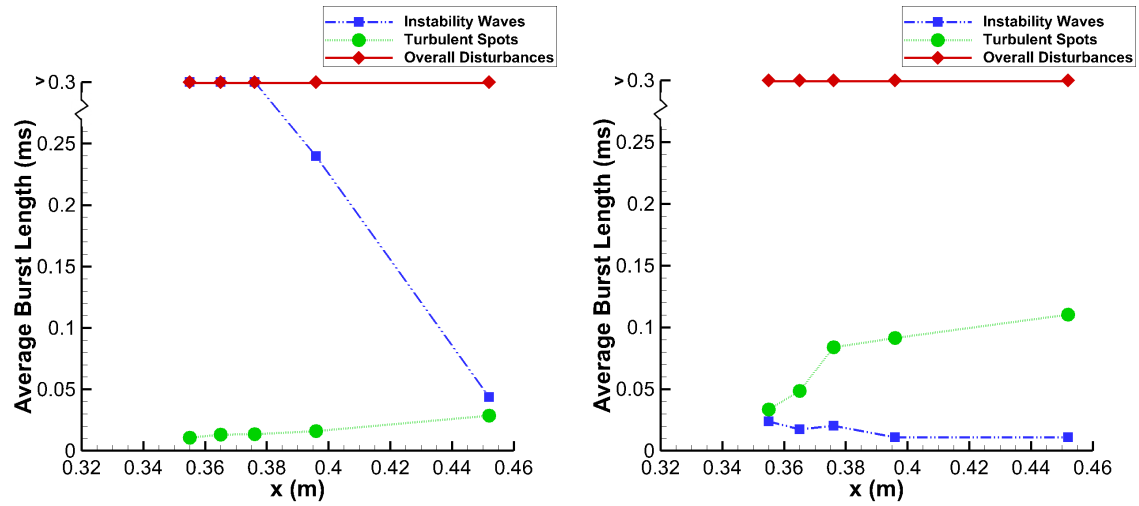

Figure 19. Average burst length along cone computed from pressure measurements, HWT-8 (a) $Re = 7.1 \times 10^6/m$**; (b)** $Re = 9.74 \times 10^6/m$**.**

IV. Concluding Remarks

Simultaneous high-frequency pressure and schlieren measurements were made of boundary-layer disturbances on a 7° cone in the Sandia Hypersonic Wind Tunnel over a range of M and Re. These measurements allowed the intermittent behavior of the boundary layer to be studied. Results highlighted how the transitional character of the boundary layer changes at higher Mach number from regions of isolated disturbances to a transitional region dominated by instability waves that then break down to turbulence.

Algorithms to distinguish instability waves from turbulent spots were developed. A wavelet analysis technique was used in the pressure measurements to separate periodic instability waves from turbulent spots with broadband components and larger low-frequency content. A different procedure was created for the schlieren measurements using a boundary-layer thickness criteria to mark turbulent regions and a correlation technique to identify instability waves. The intermittency of each region was then computed from both methods. The burst rate and average burst length was also computed from the pressure measurements.

A lot of work remains to refine and develop these techniques. The amplitude thresholds were set based on a comparison to the pressure traces and showed a dependence with Re. These thresholds appear to work well, but should be used and tested on additional Re. A sensitivity analysis remains to be done to show the effect of the chosen thresholds on the resulting transitional statistics.

Despite the ongoing work in developing these techniques, the results show the changing character of the transition region as Mach number is increased. Mach 5 results were qualitatively similar to low-speed results since isolated disturbances were observed within an otherwise laminar boundary layer. The intermittency curves for turbulent spots showed the expected error-function shape. The burst rate peaked mid-way through transition, and the average length of the turbulent spots also increased through transition as expected. However, the presence of isolated instability waves in the transition region was a clear distinction from low-speed behavior.

At Mach 8, the boundary-layer character was clearly different. Second-mode waves dominated the flow before regions of the waves broke down to turbulence. These waves were accompanied by significant pressure fluctuations which must be considered in a transitional model for pressure fluctuations in high-speed flow. The prevalence of the instability waves is an added consideration when modeling the transitional boundary layer at high M. The turbulent spot model of the transition process is occurring within regions of instability waves instead of a smooth, laminar boundary layer. If this intermittent character of the instability waves and turbulent spots can be incorporated into models, then the transitional pressure fluctuations should be able to be more accurately captured than by using a method that only distinguishes turbulent/non-turbulent regions.

Acknowledgments

Wavelet software was provided by C. Torrence and G. Compo, and is available at URL: http://paos.colorado.edu/research/wavelets/.[28]

References

[1]Laganelli, A. L., Martellucci, A., and Shaw, L. L., "Wall Pressure Fluctuations in Attached Boundary-Layer Flow," *AIAA Journal*, Vol. 21, No. 4, 1983, pp. 495–502.

[2]Pate, S. R. and Brown, M. D., "Acoustic Measurements in Supersonic Transitional Boundary Layers," AEDC-TR-69-182, October 1969.

[3]Johnson, R. I., Macourek, M. N., and Saunders, H., "Boundary Layer Acoustic Measurements in Transitional and Turbulent Flow at $M_\infty = 4.0$," AIAA Paper 69-344, April 1969.

[4]Cassanto, J. M. and Rogers, D. A., "An Experiment to Determine Nose Tip Transition with Fluctuating Pressure Measurements," *AIAA Journal*, Vol. 13, No. 10, October 1975, pp. 1257–1258.

[5]Martellucci, A., Chaump, L., Rogers, D., and Smith, D., "Experimental Determination of the Aeroacoustic Environment about a Slender Cone," *AIAA Journal*, Vol. 11, No. 5, 1973, pp. 635–642.

[6]Pate, S. R., "Dominance of Radiated Aerodynamic Noise on Boundary-Layer Transition in Supersonic/Hypersonic Wind Tunnels," AEDC-TR-77-107, March 1978.

[7]Johnson, C. B., Stainback, P. C., Wicker, K. C., and Boney, L. R., "Boundary-Layer Edge Conditions and Transition Reynolds Number Data for a Flight Test at Mach 20 (Reentry F)," NASA TM X-2584, July 1972.

[8]Dhawan, S. and Narasimha, R., "Some Properties of Boundary Layer Flow During the Transition from Laminar to Turbulent Motion," *Journal of Fluid Mechanics*, Vol. 3, No. 4, 1958, pp. 418–435.

[9]Narasimha, R., "The Laminar-Turbulent Transition Zone in the Boundary Layer," *Progress in Aerospace Sciences*, Vol. 22, January 1985, pp. 29–80.

[10]Farabee, T. M., Casarella, M. J., and DeMetz, F. C., "Source Distribution of Turbulent Bursts During Natural Transition," Tech. Rep. SAD-89E-1942, Naval Sea Systems Command, August 1974.

[11]Vinod, N., "The Signature of Laminar Instabilities in the Zone of Transition to Turbulence," *Journal of Turbulence*, Vol. 8, No. 2, 2007.

[12]Zharov, V. A., Htun, H., and Khlopkov, Y. I., "Statistical Modeling of the Turbulent Transition in the Boundary Layer," *Journal of Applied Mechanics and Technical Physics*, Vol. 50, No. 5, 2009, pp. 742–746.

[13]Park, S. and Lauchle, G., "Wall Pressure Fluctuation Spectra Due to Boundary-Layer Transition," *Journal of Sound and Vibration*, Vol. 319, 2009, pp. 1067–1082.

[14]Mee, D. J. and Goyne, C. P., "Turbulent Spots in Boundary Layers in a Free-Piston Shock-Tunnel Flow," *Shock Waves*, Vol. 6, Springer-Verlag, June 1996, pp. 337–343.

[15]Mee, D. J., "Boundary-Layer Transition Measurements in Hypervelocity Flows in a Shock Tunnel," *AIAA Journal*, Vol. 40, No. 8, 2002, pp. 1542–1548.

[16]Casper, K. M., Beresh, S. J., Wagnild, R. M., Henfling, J. F., and Spillers, R. W., "Simultaneous Pressure Measurements and Schlieren Imaging of Disturbances in a Hypersonic Boundary Layer," AIAA Paper 2013-2739, June 2013.

[17]Casper, K., *Pressure Fluctuations Beneath Turbulent Spots and Instability Wave Packets in a Hypersonic Boundary Layer*, Ph.D. Thesis, Purdue University School of Aeronautics & Astronautics, August 2012.

[18]Casper, K. M., *Hypersonic Wind-Tunnel Measurements of Boundary-Layer Pressure Fluctuations*, Master's Thesis, Purdue University, School of Aeronautics & Astronautics, August 2009.

[19]Casper, K. M., Beresh, S. J., Henfling, J. F., Spillers, R. W., Pruett, B. O. M., and Schneider, S. P., "Hypersonic Wind-Tunnel Measurements of Boundary-Layer Pressure Fluctuations," AIAA Paper 2009-4054, June 2009.

[20]Alba, C. R., Casper, K. M., Beresh, S. J., and Schneider, S. P., "Comparison of Experimentally Measured and Computed Second-Mode Disturbances in Hypersonic Boundary-Layers," AIAA Paper 2010-897, January 2010.

[21]Casper, K. M., Beresh, S. J., Henfling, J. F., Spillers, R. W., and Pruett, B. O. M., "High-Speed Schlieren Imaging of Disturbances in a Transitional Hypersonic Boundary Layer," AIAA Paper 2013-0376, January 2013.

[22]Beresh, S. J., Henfling, J. F., Spillers, R. W., and Pruett, B. O. M., "Fluctuating Wall Pressures Measured beneath a Supersonic Turbulent Boundary Layer," *Physics of Fluids*, Vol. 23, 075110, 2011.

[23]Berridge, D. C., *Measurements of Second-Mode Instability Waves in Hypersonic Boundary Layers with a High-Frequency Pressure Transducer*, Master's Thesis, Purdue University School of Aeronautics & Astronautics, December 2010.

[24]Ward, C. A. C., Wheaton, B. M., Chou, A., Berridge, D. C., Letterman, L. E., Luersen, R. P. K., and Schneider, S. P., "Hypersonic Boundary-Layer Transition Experiments in the Boeing/AFOSR Mach-6 Quiet Tunnel," AIAA Paper 2012-0282, January 2012.

[25]Ching, C. Y. and LaGraff, J. E., "Measurements of Turbulent Spot Convection Rates in a Transitional Boundary Layer," *Experimental Thermal and Fluid Science*, Vol. 11, 1995, pp. 52–60.

[26]Hedley, T. B. and Keffer, J. F., "Turbulent/Non-Turbulent Decisions in an Intermittent Flow," *Journal of Fluid Mechanics*, Vol. 64, 1974, pp. 625–644.

[27]Jordan, D., Miksad, R. W., and Powers, E. J., "Implementation of the Continuous Wavelet Transform for Digital Time Series Analysis," *Review of Scientific Instruments*, Vol. 68, No. 3, March 1997, pp. 1484–1494.

[28]Torrence, C. and Compo, G. P., "A Practical Guide to Wavelet Analysis," *Bulletin of the American Meteorological Society*, Vol. 79, No. 1, 1998, pp. 61–78.

[29]Kegerise, M.A. amd Spina, E. F., Garg, S., and Cattafesta, L. N., "Mode-Switching and Nonlinear Effects in Compressible Flow Over a Cavity," *Physics of Fluids*, Vol. 16, No. 3, March 2004, pp. 678–687.